Characterizing Local High-Frequency Solar Variability and its Impact to Distribution Studies*

Matthew Lave[a,**], Matthew J. Reno[b], Robert J. Broderick[b]

[a]*Sandia National Laboratories, 7011 East Avenue, Livermore, CA 94550, United States*
[b]*Sandia National Laboratories, 1515 Eubank SE, Albuquerque, NM 87123, United States*

Abstract

Accurately representing the local solar variability at timescales relevant to distribution grid operations (30-seconds and shorter) is essential to modeling the impact of solar photovoltaics (PV) on distribution feeders. Due to a lack of available high-frequency solar data, some distribution grid studies have used synthetically-created PV variability or measured PV variability from a different location than their study location. In this work, we show the importance of using accurate solar PV variability inputs in distribution studies. Using high-frequency solar irradiance data from 10 locations in the United States, we compare the ramp rate distributions at the different locations, use a quantitative metric to describe the solar variability at each location, and run distribution simulations using representative 1-week samples from each location to demonstrate the impact of locational solar variability on the number of voltage regulator tap change operations. Results show more than a factor of 3 difference in the number of tap change operations between different PV power variability samples based on irradiance from the different locations. Errors in number of tap changes of up to -70% are found when using low-frequency (e.g., 15-minute) solar variability.

1. Introduction

Understanding the impact of interconnecting solar photovoltaics (PV) on a distribution electric grid is crucial to maintaining the integrity of the electric grid. Underestimating the effects of PV can lead to grid damage and blackouts, while overestimating the PV impact will unduly limit the installations of this renewable energy resource. The main concern about PV interconnection is that PV is a variable generation resource; its output is not constant and depends on the amount of incident solar radiation. This variability can lead to voltage fluctuations which cause increased use of regulation equipment (e.g., on-load tap changers) and therefore increased grid maintenance costs [1].

To understand the impact of PV, it is necessary to understand the local high-frequency solar variability. High-frequency (30-second resolution or better) data on solar variability is critical since tap changers typically have time constants shorter than 1-minute, some as short as 30-seconds. High-frequency solar variability has been quantified at a few specific locations previously: Woyte, et al. [2] used up to 1-second irradiance measurements in Germany and Belgium; Perez, et al. [3] used the 20-second measured irradiance data from the ARM network in northern Oklahoma and southern Kansas; Lave, et al. [4] used 1-second irradiance measurements from a network in San Diego; and Hinkelman [5] used 1-second measured irradiance data from Oahu, Hawaii.

Understanding the solar variability at a few select locations, though, may not be helpful to an operator whose distribution grid is not located near one of these known locations. To create more high-frequency data, some studies have taken widely available low-frequency data and downscaled it to represent high-frequency data. Wegener, et al. [6]; Hansen, et al. [7]; and Hummon, et al. [8]; [9] have all presented methods for producing high-frequency data from low-frequency measurements. However, it is not clear that these downscaling methods will be accurate for distribution-scale applications, as they were not intended for ([7] and [8]) or were not well-validated at ([6] and [9]) 30-second and shorter timescales.

The lack of representative, high-frequency solar variability samples has led some distribution simulations to use synthetically-created solar variability profiles or measured solar variability from a different location than the location of the distribution feeder under study. Godfrey et al. [10] assumed a synthetic PV power ramp of 10 % per second as representative of cloud transients, but did not provide a physical justification for this ramp

*Published in *Solar Energy*, Volume 118, August 2015, Pages 327-337, ISSN 0038-092X, http://dx.doi.org/10.1016/j.solener.2015.05.028.

**Corresponding author. Tel.: +1 9252944676
Email address: mlave@sandia.gov (Matthew Lave)

[1]Sandia National Laboratories is a multi-program laboratory managed and operated by Sandia Corporation, a wholly owned subsidiary of Lockheed Martin Corporation, for the U.S. Department of Energy's National Nuclear Security Administration under contract DE-AC04-94AL85000. SAND2014-16368 J

rate. While that study focused on communications to dispatch distributed storage units, they do mention that such a profile would lead to a shortened life for the tap changer and possible voltage quality issues on the feeder. Quiroz and Reno [11] used irradiance data from southern Colorado for study of a feeder in central Utah. The irradiance was scaled to account for the different intensity of clear-sky irradiance between the two locations, and shifted to represent the accurate sunrise and sunset times in Utah. In both studies, since measured data was not available at the feeder being studied, there was no way to know if the variability profiles used were representative of the actual variability.

The focus of this work is to show the importance of using representative solar variability inputs when running distribution grid simulations. In a related study, Bank and Mather [12] differentiated between clear and cloudy days, and overall found that tap change operations were higher on the clear days due to the larger magnitude of PV power.

We explore the impact of different solar variability profiles collected at different locations on tap change operations. The 10 locations across the United States with measured high-frequency irradiance that were used for this study are described in Section 2. Section 3 discusses the ramp rate definition we used and shows the ramp rate distributions for each of the locations. In Section 4, we propose a variability metric that is useful for quantifying high-frequency variability and use it compare both the annual and daily variability between the different locations. Section 5 presents results of distribution feeder simulations to determine the number of tap change operations caused by sample PV profiles for each of the 10 locations. Finally, in Section 6, we present the conclusions describing the importance of using representative solar inputs.

2. High-Frequency Data

We assembled a database of high-frequency (time resolution of 30-seconds or better) global horizontal irradiance (GHI) measurements from 10 different locations in the United States. We chose to use GHI data to allow for direct comparisons between the different locations. Plane of array (POA) irradiance measurements with varying tilts would make comparisons between sites impractical.

The site locations are shown on a map in Fig. 1, and details about the date ranges of available data and time resolution of the data are listed in Table 1. Albuquerque (PSEL) was collected at Sandia National Laboratories while Albuquerque (Mesa) was collected approximately 10 km southwest. These two sites will allow for validation of methods, as similar results should be obtained for each site due to their close proximity.

As close to one year of data as possible was used to capture all seasonal trends. The Albuquerque Mesa and Lanai sites only had 11 months of data, but are still

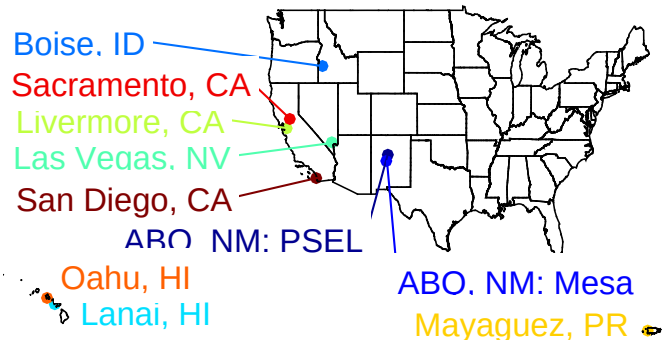

Figure 1: Map of high-frequency data.

Table 1: Data description.

Location	Data Used	Time Res.
Albuquerque, NM (PSEL)	2/2013 - 12/2013	3s
Albuquerque, NM (Mesa)	2/2013 - 12/2013	1s
Boise, ID	5/2013 - 4/2014	10s
Lanai, HI	2/2010 - 12/2010	1s
Las Vegas, NV	1/2010 - 12/2010	1s
Livermore, CA	12/2013 - 11/2014	2s
Mayaguez, PR	9/2012 - 8/2013	1s
Oahu, HI	3/2010 - 2/2011	1s
Sacramento, CA	1/2012 - 12/2012	30s
San Diego, CA	1/2011 - 12/2011	1s

expected to be representative of annual trends. The Albuquerque PSEL site has a long period of record, but data was only used from days when data was also available at the Albuquerque Mesa site to allow for direct comparisons between the two Albuquerque sites. The Mayaguez site had intermittent data outages lasting up to two months, so may not be fully representative of annual trends. However, since our goal in this work is show how variability differences *can* impact distribution feeders, we include Mayaguez in our analysis.

3. Ramp Rate Distributions

Using the collected high-frequency data, we first computed irradiance ramp rates (RRs). We chose to look in detail at the 30-second RRs since tap changers on distribution feeders can have time constants as short at 30-seconds.

There has been some debate as to what definition of ramp rate is best for PV variability studies. Some authors have defined ramp rates as the instantaneous differences in power output separated by the timescale of interest, normalized by the timescale (e.g., Eq. 1 in [13]). Others have looked at the magnitude and duration of ramps using assumed tolerances (minimum time offset from previous ramp and minimum magnitude) for defining individual ramps (e.g., Fig. 1 in [14]).

The data used in this study varies in time resolution from 1-second to 30-seconds (Table 1). Due to data collection methods, the longer time resolution data represents averages over the time interval. For example, to create the 30-second data recorded in Sacramento, the irradiance sensor sampled at 1 Hz, then once every 30-seconds the average irradiance over the past 30-seconds was recorded. Because of this, neither the instantaneous differences nor the magnitude and duration methods will produce consistent ramp rates over the different resolutions of measured data: if data at the same location were recorded at both 1-second and 30-second intervals, different 30-second ramps would be computed from the two different resolution timeseries. Therefore, we chose to use the moving averages definition of ramp rates (Eq. 7.1 in [15]):

$$RR^{Irr}_{\Delta t}(t) = \frac{1}{\Delta t}\left(\sum_{t}^{t+\Delta t} Irr - \sum_{t-\Delta t}^{t} Irr\right), \quad (1)$$

where $RR^{Irr}_{\Delta t}(t)$ is the irradiance ramp rate for timescale Δt at time t. This definition is consistent across the different data time resolutions since the 30-second ramps are the differences between 30-second averages of the data.

From the irradiance ramp rates computed using Eq. 1, we computed the annual distribution of ramp rates for the irradiance data at each location. Only ramps that occurred when the solar altitude angle was greater than 10° were included, to filter out nighttimes and times of very low solar altitude angles when the irradiance sensors are prone to higher angular response errors. Additionally, we used only the magnitude not the sign of the ramps, which is common practice since positive and negative ramps typically have similar probabilities of occurrence. The 30-second distributions of ramp rates are shown in Fig. 2. Note that the y-axis is $P(RR > RR_0)$, which is the inverse of typical cumulative distribution functions (cdfs) that describe $P(RR \leq RR_0)$, but allows for easier readability of extreme ramp rate magnitudes.

The cumulative distributions show that, for example, only 3% of ramp rates in Sacramento were larger than 50 W m^{-2} in 30-seconds (labeled 5% in Fig. 2), but that 20% of ramp rates in Oahu were larger than 50 W m^{-2} in 30-seconds.

4. Quantifying Solar Variability Based on Ramp Rate Distributions

4.1. VS_{RRdist} Variability Metric Definition

The RR distributions presented in Section 3 are useful for understanding the probability of occurrence of specific magnitudes of ramp rates, but it is difficult to quantitatively compare one location to another. Since large magnitude ramps which occur frequently have the largest impact on grid operations, we propose a metric called the variability score from the RR distribution, VS_{RRdist}, which is defined as the maximum value of ramp rate magnitude (RR_0) times ramp rate probability, scaled by 100 to allow for easier to interpret values (i.e., whole numbers rather than decimals):

$$VS_{RRdist}(\Delta t) = 100 \times max[RR_0 \times P(|RR_{\Delta t}| > RR_0)]. \quad (2)$$

In Eq. 2, RR_0 ranges from the minimum to the maximum ramp rate. RR_0 is either a percent of $1000 W m^{-2}$ (STC irradiance) for irradiance ramps, or a percent of rated capacity for power ramps. The probability $P(|RR_{\Delta t}| > RR_0)$ is expressed as a percent.

For example, for the Oahu distribution shown in Fig. 2, the maximum ramp rate magnitude times probability occurred when $RR_0 = 20.0\%$ and $P(|RR^{GHI}_{30s}| > RR_0) = 8\%$, thus combining for a maximum value of 1.6%. With the scaling factor of 100 in Eq. 2, this becomes 160%. However, since the % was a combination of two different units (% of capacity ramp rate and probability of ramp rate), it does not have physical meaning and so we choose to drop it. Therefore, for the annual distribution of ramp rates at Oahu, $VS^{GHI}_{RRdist}(30s) = 160$.

Following the definitions in paragraphs, VS_{RRdist} range from 0 (no variability) to 10000 (all ramps are 100% of capacity). Larger VS_{RRdist} values indicate more variability.

We note that our choices of scaling factor and expressing the ramp magnitudes and probabilities in percentages do not impact our comparison of VS_{RRdist}. If using a different scaling factor or using decimals instead of percentages, the range of possible VS_{RRdist} values would change but the relative differences between VS_{RRdist} values would stay the same.

The VS_{RRdist} metric is based directly on the ramp rates in irradiance or power. While other works (e.g., [16]

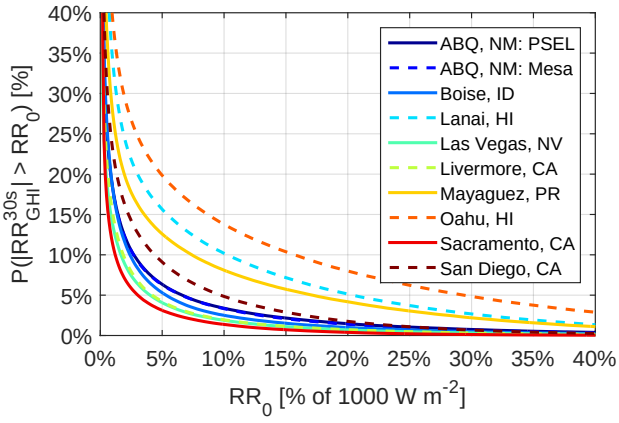

Figure 2: 30-second cumulative distributions of GHI ramp rates from 1-year of data at each location.

and [4]) have examined the variability of the clearness (irradiance normalized by extraterrestrial irradiance) or clear-sky index (irradiance normalized by expected clear-sky irradiance on the Earth's surface), they did so to remove the diurnal and seasonal cycles to focus on understanding cloud-caused fluctuations. In this work, since we address the impact of solar variability to the electric grid, diurnal and seasonal fluctuations are important and must not be eliminated. For example, a clear-sky index change of 0.5 in the early morning in winter will have a much smaller impact on PV power production and hence electric grid operations than a clear-sky index change of 0.5 midday in the summer. Thus, all variability analysis presented here is based on irradiance or power output directly rather than normalized values.

4.2. Annual $VS^{GHI}_{RRdist}(30s)$ at each Location

Based on the distributions of 30-second GHI ramp rates over 1-year (Fig. 2), the ramp rate magnitudes times probabilities are shown in the left side of Fig. 3. The maximum value of each ramp rate magnitude times probability curve is the $VS^{GHI}_{RRdist}(30s)$ based on the annual distribution of ramp rates at that location; these are shown in the bar chart on the right of Fig. 3. The $VS^{GHI}_{RRdist}(30s)$ values are consistent with typical weather patterns: Sacramento, Las Vegas, and Livermore (sunny locations) are the least variable, while the island locations of Oahu, Mayaguez, and Lanai (which are often partly cloudy) are the most variable. The two Albuquerque sites have very similar VS_{RRdist} values, as expected due to their close proximity.

4.3. VS^{GHI}_{RRdist} Variation with Timescale

GHI ramp magnitudes vary with timescale [4]: as the timescale increases, so do the ramp magnitudes due to the longer time interval over which solar irradiance can deviate from its previous value. Since VS_{RRdist} is based on ramp rate distributions, VS_{RRdist} values are also expected to increase with increasing timescale. To examine this behavior, we calculated ramp rates using Eq. 1 at timescales Δt = 1s, 10s, 30s, 60s, and 3600s for each location with sufficient temporal resolution (e.g., Sacramento had only 30-second resolution so 1-second and 10-second ramp rates could not be resolved). From annual distributions of ramp rates at these various timescales, we used Eq. 2 to compute VS^{GHI}_{RRdist} for each location and timescale pair, as shown in Fig. 4.

For all locations, VS^{GHI}_{RRdist} increases with increasing timescale. At all timescales, the ranking of locations from least variable to most variable is similar. For the 1-second, 10-second, 30-second, and 60-second timescales, VS^{GHI}_{RRdist} values vary by approximately a factor of 10 from the least variable location (Las Vegas or Sacramento) to the most variable location (Oahu). At the 1-hour timescale, ramps become dominated by

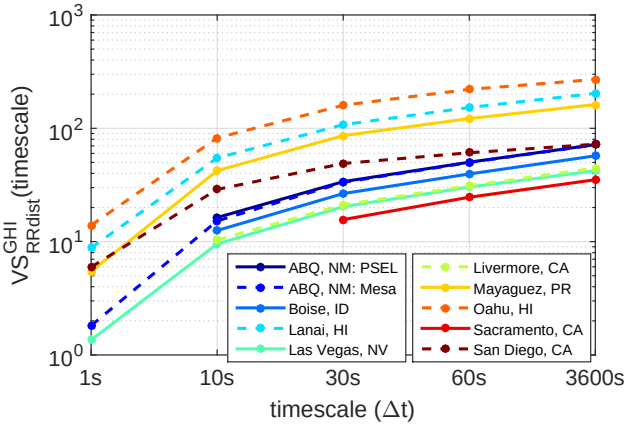

Figure 4: Annual VS^{GHI}_{RRdist} values for each location over RR timescales Δt = 1s, 10s, 30s, 60s, and 3600s. Values are not plotted for timescales/location pairs without sufficient temporal resolution (see Table 1).

diurnal effects of the sun rising and setting rather than the cloud-caused fluctuations that dominated at shorter timescales. Thus, there is less spread by location in the $VS^{GHI}_{RRdist}(3600s)$ values since all locations experience similar diurnal cycles as they are all at mid-latitudes (latitudes range from 18.2°N to 43.6°N).

4.4. Daily $VS^{GHI}_{RRdist}(30s)$ Examples and Distributions

While sections 4.2 and 4.3 present VS_{RRdist} values computed from annual distributions of ramp rates, Eqn. 2 can also be applied to daily distributions of ramp rates to quantify daily variability. Just as for the annual distributions, only ramps that occurred when the solar altitude angle was greater than 10° were included in the daily distributions.

Fig. 5 shows the daily distributions of ramp rates for all 365 days considered at Oahu, color coded by their daily $VS^{GHI}_{RRdist}(30s)$ values. The annual distribution of ramp rates (from Fig. 2) is also included for direct comparison. The gradient of low to high daily $VS^{GHI}_{RRdist}(30s)$ values from the bottom left to top right of the plot is distinct and is consistent with an intuitive ranking of variability: distributions with higher probabilities of large ramps (distributions towards the top right) should have higher variability scores.

To compare the daily variability between the locations, Fig. 6 shows histograms of daily $VS^{GHI}_{RRdist}(30s)$ values at each location. Also included in Fig. 6 are black dashed lines showing the annual $VS^{GHI}_{RRdist}(30s)$ values to demonstrate how the daily values deviate from the annual value. The locations with low annual $VS^{GHI}_{RRdist}(30s)$ scores had many daily $VS^{GHI}_{RRdist}(30s)$ scores between 0 and 50, indicating many mostly or fully clear days. At Oahu, daily $VS^{GHI}_{RRdist}(30s)$ values follow a nearly uniform distribution, especially for $VS^{GHI}_{RRdist}(30s)$ values between 0 and 300. Lanai and Mayaguez had peaked distributions, with values between 100 and 150 at

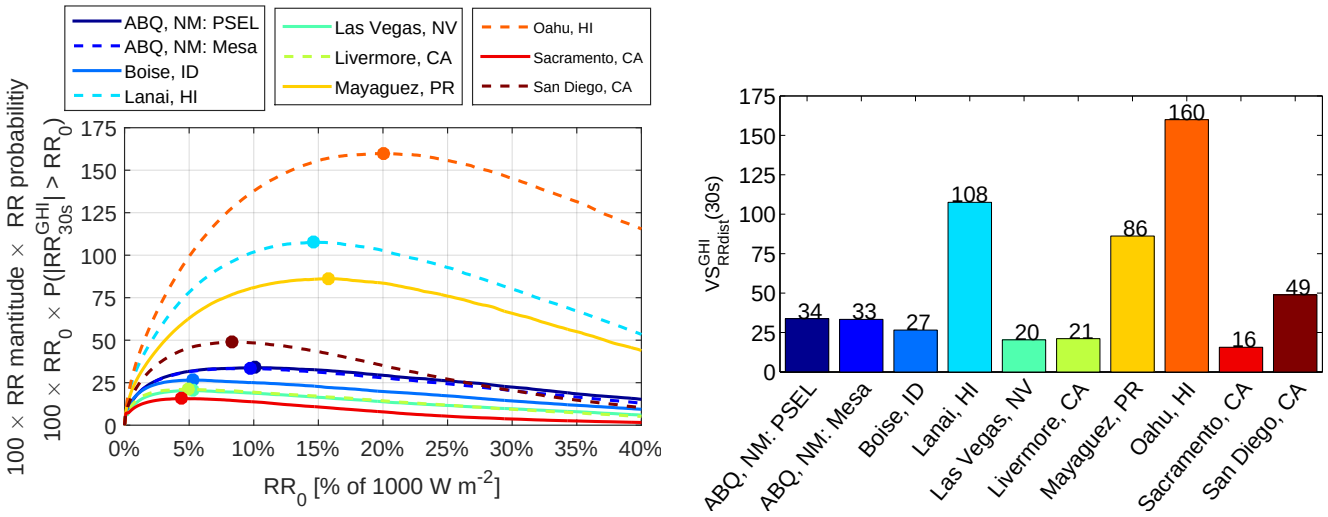

Figure 3: (Left) Ramp rate magnitudes times probabilities for annual distributions of 30-second GHI ramp rates, with dots marking maximum values. These maximum values are the annual $VS^{GHI}_{RRdist}(30s)$ values, which are re-plotted in the bar chart (Right) for visual comparison.

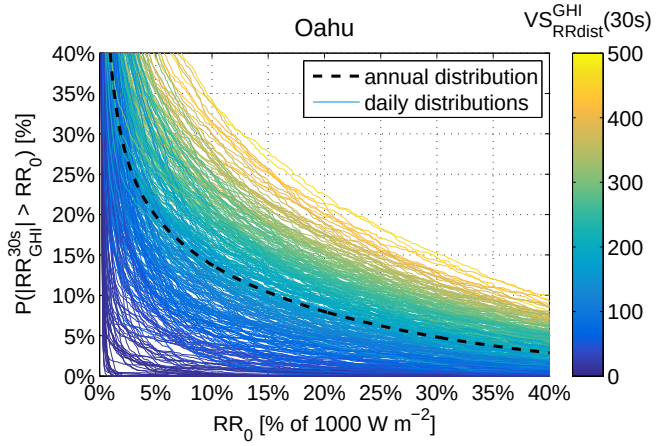

Figure 5: Daily 30-second cumulative distributions of GHI ramp rates at Oahu. The colors of each distribution indicate the daily $VS^{GHI}_{RRdist}(30s)$ value. The annual distribution (as in Fig. 2) is included as the black dashed line for reference.

Lanai and between 50 and 100 at Mayaguez occurring most often.

4.5. VS_{RRdist} Compared to the Variability Index

The variability index (VI) [17] is an established metric used to compare variability over different days, and it can also be applied to compare variability at different locations. The VI is calculated as:

$$VI(\Delta t) = \frac{\sum_t \sqrt{RR^{GHI}_{\Delta t}(t)^2 + \Delta t^2}}{\sum_t \sqrt{RR^{CSI}_{\Delta t}(t)^2 + \Delta t^2}}, \quad (3)$$

where CSI is the calculated clear-sky irradiance. To ensure that the VS_{RRdist} metric defined here is reasonable, Fig. 7 shows a scatter plot of daily $VS^{GHI}_{RRdist}(30s)$ versus daily VI(30s). The high correlation between VI and VS_{RRdist} (Pearson correlation coefficient = 0.99) confirms that VS_{RRdist} is consistent with VI at quantifying the variability.

Even though VS_{RRdist} and VI are consistent, we feel that VS_{RRdist} is an improvement over VI due to its simplicity. The VI requires a clear-sky model to compute the clear-sky irradiance. While GHI clear-sky models are common and validation has shown good performance [18], fixed tilt and single-axis tracking clear-sky models are significantly more complicated and are not well-validated. Further complexity arises in creating clear-sky models of power output, due to the added variables of soiling, tracking algorithms, failures, etc. Since VS_{RRdist} is computed directly from the ramp rate distribution, it does not require a clear-sky model and so can be just as easily applied to POA, tracking, and power timeseries as it can to GHI timeseries. Though, as discussed in section 5.1, the VS_{RRdist} computed from GHI will be different from the VS_{RRdist} computed from POA or power, even at the same location.

5. Impact to Distribution Grid

In Sections 3 and 4, we computed statistics describing the variability of GHI at each location. However, GHI variability does not directly determine the impact of PV variability to the distribution grid. In this section, we use sample weeks of PV power output created from irradiance samples at each location to determine the effect of PV variability on the number of tap change operations of a voltage regulator in a detailed simulation of a real distribution system.

Since many assumptions must be made (PV size and location, feeder layout, etc.) to run distribution grid feeder simulations, the results in this section are meant to be illustrative of the impact that different irradiance

profiles can have on the number of voltage regulator tap change operations. To understand the unique impacts of different scenarios to voltage regulation equipment, simulations with the exact PV sizing and feeder layout would be required.

5.1. Weekly PV Power Samples for Distribution Studies

It was not practical to run the distribution simulations for a full year due the long amount of computer processing time required for simulations. Instead, we chose a "typical" week from each location for use in the distribution simulations. The typical week was chosen by finding the week at each location that had a ramp rate distribution with a VS^{GHI}_{RRdist} value closest to the annual VS^{GHI}_{RRdist} value. At all locations, the week chosen had a VS^{GHI}_{RRdist} value within 0.5% of the annual VS^{GHI}_{RRdist} value.

Using the week selected at each location, the irradiance was used to model the power output of a 3MW single-axis tracking PV power plant. This was done by:

1. smoothing the point sensor GHI based on the spatial coverage of a 3MW PV plant (~18.5 acres) to determine the plant-average GHI using the wavelet variability model (WVM) [19], with cloud speeds chosen as in [20]
2. translating the plant-average GHI to represent plant-average POA irradiance incident on a single-axis tracking plane using the Hay and Davies transposition model [21]
3. converting the plant-average POA irradiance to AC power output using the Sandia Array Performance Model [22] and the Sandia Inverter Performance Model [23].

The weekly power output samples for each location are shown in Fig. 8. Consistent with their low VS^{GHI}_{RRdist} values, Las Vegas, Livermore, and Sacramento all had multiple clear days in their weekly samples. Conversely, Lanai, Oahu, and Mayaguez, all locations with high VS^{GHI}_{RRdist} values, had many highly variable days in their sample weeks.

The weekly samples shown in Fig. 8 are *power*, not GHI. The steps used to convert the measured point sensor GHI to 3MW single-axis tracking PV plant power output all affect the variability. The spatial smoothing over the plant will reduce the variability. The translation of GHI to single-axis plane of array will increase the power output, increasing the ramp rates and hence the variability. The irradiance to power conversion may slightly reduce the variability due to inverter clipping. Thus, for the power samples we must quantify the variability using VS^{power}_{RRdist}, as shown in Fig. 9.

In comparing Fig. 9 to Fig. 3, we see that $VS^{power}_{RRdist} < VS^{GHI}_{RRdist}$ at all locations except Boise. This reduction in variability is mostly due to the spatial smoothing across the 3MW PV plant. In the wavelet variability model, spatial smoothing is inversely proportional to the cloud speed: slower cloud speeds mean more spatial smoothing. The locations where the reduction from VS^{GHI}_{RRdist} to VS^{power}_{RRdist} was largest were the locations with the slowest cloud speeds during sample weeks. The increase in VS_{RRdist} at Boise is due to its very fast cloud speeds (leading to little spatial smoothing), which did not provide enough smoothing to outweigh the increased variability in irradiance on a single axis tracking plane versus GHI.

Even though the two Albuquerque locations had nearly identical VS^{GHI}_{RRdist} values, they differ significantly in their VS^{power}_{RRdist} values due to different cloud speeds. The week sample chosen for the PSEL location was from July when cloud speeds are typically slow in New Mexico: the average cloud speeds for the PSEL sample week was 3.9 m/s. Conversely, the Mesa sample was from April when cloud speeds are high in New Mexico (see Fig. 7 in [20] for seasonal comparisons of cloud speeds), and the average cloud speed for the Mesa sample was 14.6 m/s.

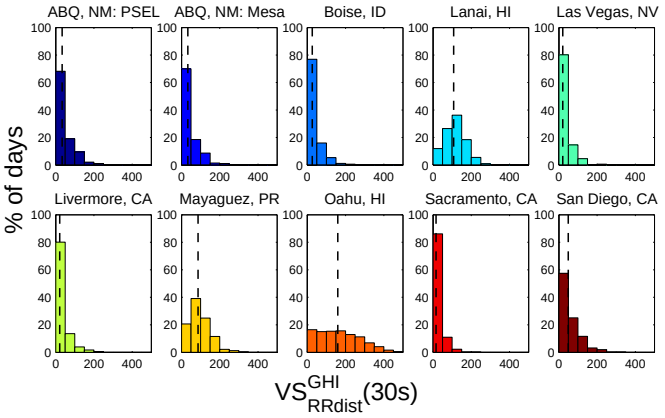

Figure 6: Histograms of daily $VS^{GHI}_{RRdist}(30s)$ values derived from the daily RR distributions at each location. The annual $VS^{GHI}_{RRdist}(30s)$ values (from Fig. 3) are included as black dashed lines for reference.

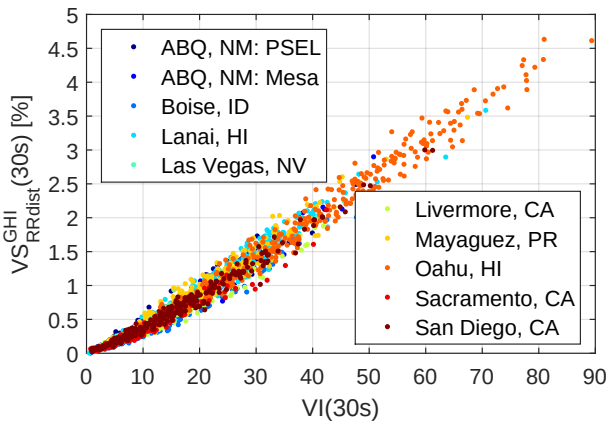

Figure 7: Scatter plot of the daily $VS^{GHI}_{RRdist}(30s)$ versus the daily 30-second variability index VI(30s).

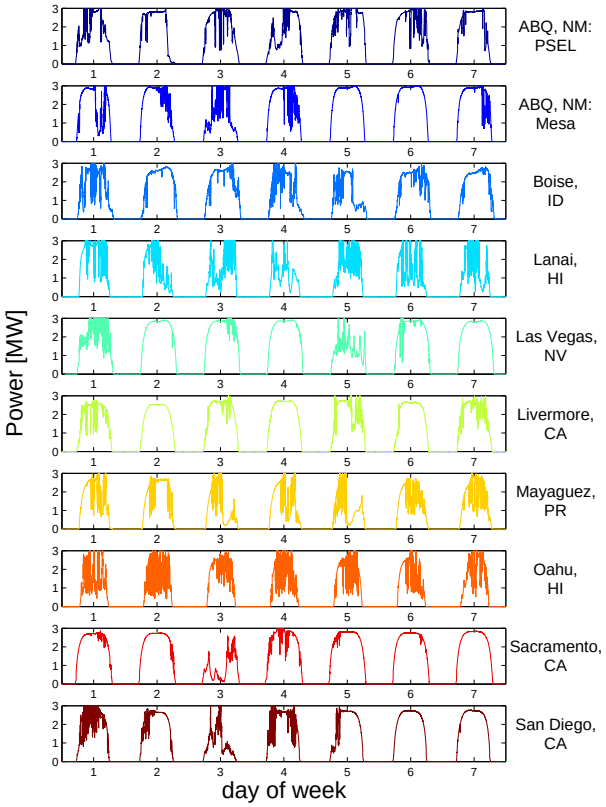

Figure 8: Sample weeks of 3MW of single-axis tracking PV power output based on irradiance samples at each location. These samples were used as input for distribution studies.

5.2. Feeder Setup

We used a 12kV agricultural feeder in California as our test feeder. The feeder layout is shown in Fig. 10. This feeder was chosen partly because of the location of its voltage regulator (approximately halfway down the feeder), which allowed for simulation of a 3MW PV plant just beyond the voltage regulator.

For all simulations, the load profile from the week with maximum load recorded at this feeder was used. Load was recorded at 30-minute intervals and linearly interpolated to 1-second for this analysis. During this maximum load week, the maximum feeder load was 8.5MW, and the minimum feeder load was 4.8MW. Through the voltage regulator, the maximum load was 4.7MW, and minimum load was 2.7MW. The variability in load was small: the largest ramp through the voltage regulator was 0.25MW in 30 minutes, and the $VS^{load}_{RRdist}(30s) = 0.9$ for the load through the voltage regulator, which is much smaller than the VS^{power}_{RRdist} values shown in Fig. 9. Based on this load profile, we chose to simulate a 3MW PV plant since this was approximately the maximum amount of PV that would not lead to reverse flow through the regulator. The PV power output profile varied for each simulation, as shown in Fig. 8.

Using the distribution simulation program OpenDSS coupled with the analysis program MatLab [24], quasi-static time-series (QSTS) power flow analyses at 1-second resolution were computed. PV variability samples were linearly interpolated to 1-second for locations that did not have 1-second variability samples (Tabel 1). This is expected to have a minimal effect on results since the temporal resolution at each location was always shorter than the voltage regulator time constant. The analysis was run 11 different times: once with no PV as a base case, and once for each of the 10 different PV power profiles. The voltage regulator was simulated using the default OpenDSS control [25] and had a time delay of 45s in all simulations, consistent with the actual feeder setup.

5.3. Voltage Regulator Operations

The distribution grid impact analysis focused on the number of times the line voltage regulator changed taps

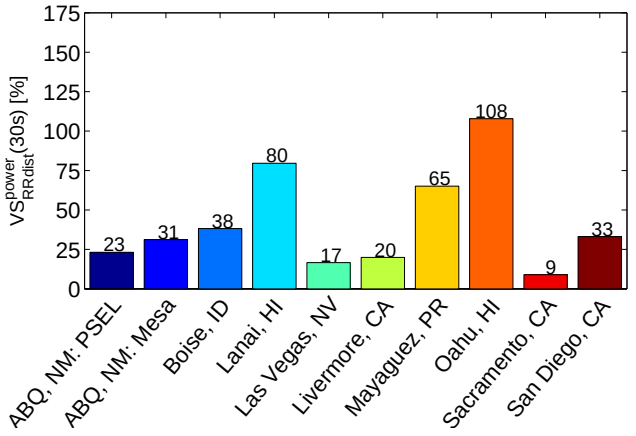

Figure 9: Bar chart of $VS^{power}_{RRdist}(30s)$ derived from the ramp rate distributions of the weekly power samples shown in Fig. 8.

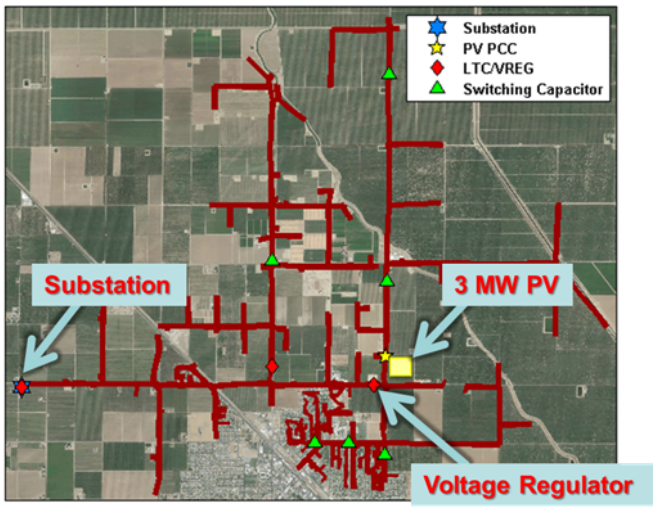

Figure 10: Layout of the study distribution feeder showing the location of the substation, the voltage regulator considered, and the 3MW of PV.

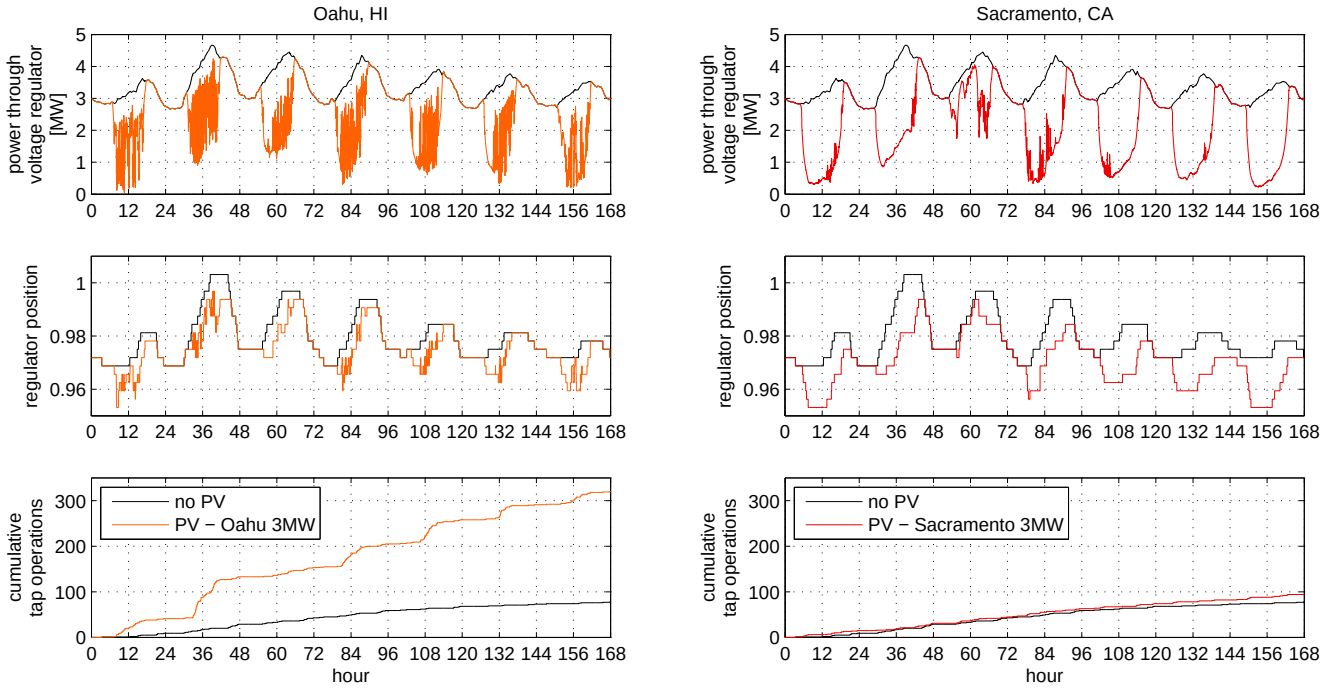

Figure 11: Power through voltage regulator (top), voltage regulator tap position (middle), and cumulative number of tap changes (bottom) for the feeder base case with no PV (black, both plots) and for the 3MW Oahu, HI test case (orange, left plots), and for the 3MW Sacramento, CA test case (red, right plots).

in order to keep the feeder voltage in normal range. Increased tap changes lead to increased operation and maintenance costs and reduce the lifetime of the regulator. Fig. 11 shows the results of the QSTS analysis for the base case and for the Oahu and Sacramento PV power profiles. The power through the voltage regulator in the no PV base case (black line in top plots in Fig. 11 is the load profile. The week starts on a Sunday (hours 0-24) and ends on a Saturday (hours 144-168), and both of these weekend days had lower load than during the weekdays. As a result, the voltage regulator did not change its position very often when no PV was connected, and so there were relatively few tap changes. Monday (hours 24-48) was the day with the highest load, and also had 20 tap change operations in the no PV case, the most of any day. It is important to remember that voltage regulators were traditionally installed to regulate load, so there can be a significant amount of tap change operations even without PV. Over the whole week, there were 78 tap change operations in the no PV base case.

When using the Oahu PV power sample, the power through the regulator fluctuated much more than in the no PV case. On Monday (hours 24-48), the high PV variability combined with the high load caused a total of 92 tap changes on that one day. Since nearly every day had high variability, over the entire week there were 320 tap change operations, more than four times as many as in the base case.

The Sacramento PV sample did not increase the tap change operations nearly as much as the Oahu sample. On the Monday (hours 24-48), the Sacramento PV sample produced only 16 tap operations, which is a decrease from the no PV case. This occurred because the Sacramento PV had significant production during the peak load time, such that the tap changer did not have to "chase" the load as far, while also not having much variability and so not introducing many new tap operations. On other days, the Sacramento PV variability did cause additional tap operations; over the whole week the Sacramento sample led to 94 tap changes, a modest 21% increase over the no PV case.

5.4. Tap Changes at each Location

Fig. 12 shows the total number of tap change operations in the sample week for each of the PV power profiles, including the base case with no PV. The Oahu sample by far causes the most tap changes, as it lead to a more than 300% increase in tap changes over the no PV base case. The Lanai (228%) and Mayaguez (198%) PV profiles also lead to large increases in tap operations over the base case. This is consistent with the large VS^{power}_{RRdist} and VS^{GHI}_{RRdist} values found at these locations. The Sacramento (21%) and Livermore (38%) locations resulted in only a small increase in tap change operations over the base case. Again, this is consistent with the small VS^{power}_{RRdist} and VS^{GHI}_{RRdist} values at these locations.

Other locations did not show as strong of a relationship between VS^{power}_{RRdist} and the number of tap

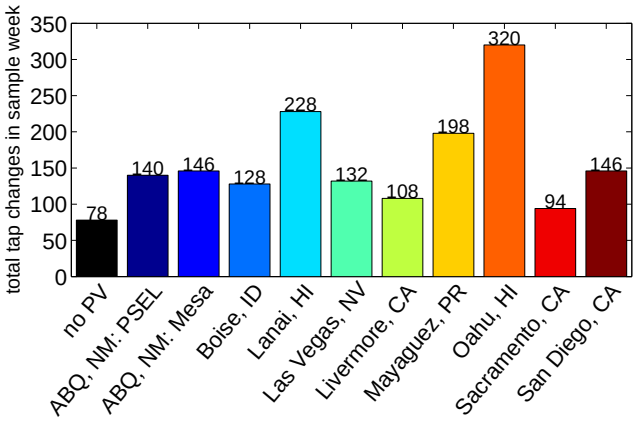

Figure 12: Total tap changes during the sample weeks when using 3MW PV variability profiles from each location. The black bar is the feeder base case with no PV.

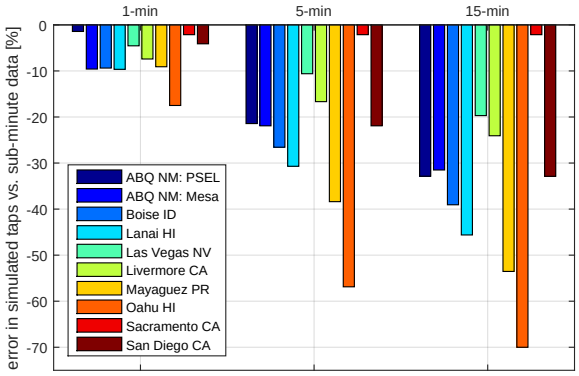

Figure 13: Percent error in tap changes when using 1-minute, 5-minute, or 15-minute resolution PV power data versus using 1-second resolution PV power data. For example, at Oahu when using 15-minute data only 96 tap change operations occurred, which is a -70% error compared to the 320 tap changes when using 1-second data.

changes. The Las Vegas sample had more tap changes than the Livermore sample, even though the Las Vegas VS^{power}_{RRdist} was lower. This difference is due to the timing of the solar fluctuations relative to the load: more of the Las Vegas variability occurred at times of low load (e.g., on Sunday, hours 0-24), and so had more of an impact on tap change operations.

5.5. Need for High-Frequency Solar Variability

To demonstrate the importance of high-frequency solar variability in simulating the impact of PV on distribution grids, we re-ran the simulations described in the previous sections using lower frequency solar variability data. For this comparison, we down sampled the 1-second power timeseries to create 1-minute, 5-minute, and 15-minute resolution power timeseries. This was done using backward-looking block averages. For example, the average of all values between (inclusive) 6:00:01 and 6:01:00 was recorded as the 1-minute data point at 6:01:00. Thus, this data is representative of sensors that collect low-frequency data in this manner: measure at high-frequency, average, then record the low-frequency average. These block-averages were linearly interpolated to 1-second in the same way that the load data was interpolated to 1-second before being fed into the distribution simulation.

Figure 13 shows the errors in the 1-minute, 5-minute, and 15-minute data at matching the number of tap change operations found with the sub-minute data. All errors were negative, meaning that the low-frequency data always under predicted the number of tap changes. For example, for the Oahu sample, 320 tap changes were found in the 1-second simulation, but only 264, 138, and 96 tap changes were found in the 1-minute, 5-minute, and 15-minute cases, respectively.

Errors were correlated with the variability at each location. The smooth Sacramento sample had very small errors even for the 15-minute resolution, presumably due to the lack of high-frequency solar variability in the sample week. Oahu, by contrast, had -17.5% error just by using 1-minute resolution data.

Except for the Oahu sample, 1-minute errors were modest ($< 10\%$) and likely within the margin of other errors (e.g., errors in modeling the feeder layout, the PV production, etc.), suggesting that 1-minute data may be acceptable for rough simulations if no higher frequency data is available. These modest 1-minute errors are likely explained by the 45-second (i.e., similar to 1-minute) time constant on the voltage regulator: a shorter voltage regulator time constant would likely result in larger errors. Errors for the 5-minute and 15-minute resolution data were significant, showing the importance of using high-frequency solar variability samples to attain accurate simulations of the impact of PV on distribution grids.

6. Conclusion

The distribution simulation results using different PV variability profiles by location have strong implications for distribution studies and PV integration. Significant overestimation or underestimation of the impact of PV can occur due to choosing an inappropriate solar variability profile. For example, a distribution study that used the Oahu irradiance profile to represent the irradiance in Sacramento would overestimate the number of tap changes by more than a factor of 3. Such a study might erroneously assign a high cost to PV integration due to increased voltage regulator operation and maintenance costs, and decreased lifetime. Conversely, a study of a distribution feeder in Oahu using PV data from Sacramento would significantly underestimate the impact on tap change operations and may assign too low of a cost to PV integration. Using low-frequency solar variability data can also cause significant

underestimation of tap change operations, such as the -70% error when using 15-minute data at Oahu.

Overall, the number of tap changes were well correlated with the PV power variability score VS^{power}_{RRdist} and even with the GHI variability score VS^{GHI}_{RRdist}. This shows that the variability score VS_{RRdist} can be a useful metric for quantifying solar variability. Variability samples with high VS_{RRdist} values (such as Oahu, Lanai, and Mayaguez) can be expected to have a large impact on voltage fluctuations, while variability samples with low VS_{RRdist} values will be expected to have less of an impact. However, variables such as PV module POA or tracking setup and geographic smoothing over the spatial area of a PV plant mean that VS^{GHI}_{RRdist} may not be a good predictor of VS^{power}_{RRdist}. Additionally, distribution grid variables such as feeder layout, tap changer settings, and load profiles mean that VS^{power}_{RRdist} may not be a good predictor of tap change operations. To understand the specific impact of PV to a distribution grid, a detailed study accounting for all of these variables is required.

Acknowledgments

Thanks to Idaho Power, SunPower Corporation, the Sacramento Municipal Utility District, and the University of California, San Diego for sharing high-frequency irradiance data. Data for Oahu was taken from the NREL Oahu Solar Measurement Grid (http://www.nrel.gov/midc/oahu_archive/).

References

[1] G. Ari, Y. Baghzouz, Impact of high pv penetration on voltage regulation in electrical distribution systems, in: Clean Electrical Power (ICCEP), 2011 International Conference on, 2011, pp. 744–748. doi:10.1109/ICCEP.2011.6036386.

[2] A. Woyte, R. Belmans, J. Nijs, Fluctuations in instantaneous clearness index: analysis and statistics, Solar Energy 81 (2) (2007) 195–206.

[3] R. Perez, S. Kivalov, J. Schlemmer, K. Hemker Jr, T. E. Hoff, Short-term irradiance variability: Preliminary estimation of station pair correlation as a function of distance, Solar Energy 86 (8) (2012) 2170–2176.

[4] M. Lave, J. Kleissl, E. Arias-Castro, High-frequency irradiance fluctuations and geographic smoothing, Solar Energy 86 (8) (2012) 2190–2199.

[5] L. M. Hinkelman, Differences between along-wind and cross-wind solar irradiance variability on small spatial scales, Solar Energy 88 (0) (2013) 192–203.

[6] J. Wegener, M. Lave, J. Luoma, J. Kleissl, Temporal downscaling of irradiance data via Hidden Markov Models on Wavelet coefficients: Application to California Solar Intiative data (2012).
URL `http://calsolarresearch.ca.gov/images/stories/documents/Sol1_funded_proj_docs/UCSD/ucsd_rpt_downscaling-1sec.pdf`

[7] C. Hansen, J. Stein, A. Ellis, Estimating annual synchronized 1-min power output profiles from utility-scale PV plants at 10 Locations in Nevada for a solar grid integration study, Tech. Rep. SAND2011-5529, Sandia National Laboratories (2011).

[8] M. Hummon, E. Ibanez, G. Brinkman, D. Lew, Sub-hour solar data for power systems modeling from static spatial variability analysis, Tech. Rep. NREL/CP-6A20-56204, National Renewable Energy Laboratory (2012).

[9] M. Hummon, A. Weekley, K. Searight, K. Clark, Downscaling solar power output to 4-seconds for use in integration studies, Tech. Rep. NREL/CP-6A20-60335, National Renewable Energy Laboratory (2013).

[10] T. Godfrey, S. Mullen, R. C. Dugan, C. Rodine, D. W. Griffith, N. Golmie, Modeling smart grid applications with co-simulation, in: First IEEE International Conference on Smart Grid Communications (SmartGridComm), 2010, pp. 291–296.

[11] J. Quiroz, M. Reno, Detailed grid integration analysis of distributed PV, in: 38th IEEE Photovoltaic Specialists Conference (PVSC), 2012, pp. 596–601.

[12] J. Bank, B. Mather, Analysis of the impacts of distribution connected PV using high-speed datasets, in: IEEE Green Technologies Conference, 2013, pp. 153–159.

[13] J. Johnson, B. Schenkman, A. Ellis, J. Quiroz, C. Lenox, Initial operating experience of the 1.2-MW La Ola photovoltaic system, in: 38th IEEE Photovoltaic Specialists Conference (PVSC), Volume 2, 2012, pp. 1–6.

[14] C. W. Hansen, J. S. Stein, A. Ellis, Statistical criteria for characterizing irradiance time series, Tech. Rep. SAND2010-7314, Sandia National Laboratories (2010).

[15] J. Kleissl, Solar energy forecasting and resource assessment, Academic Press, 2013.

[16] A. Woyte, V. Van Thong, R. Belmans, J. Nijs, Voltage fluctuations on distribution level introduced by photovoltaic systems, Energy Conversion, IEEE Transactions on 21 (1) (2006) 202–209. doi:10.1109/TEC.2005.845454.

[17] J. S. Stein, C. W. Hansen, M. J. Reno, The variability index: A new and novel metric for quantifying irradiance and PV output variability, Tech. Rep. SAND2012-288C2, Sandia National Laboratories (2012).

[18] M. J. Reno, C. W. Hansen, J. S. Stein, Global horizontal irradiance clear sky models: Implementation and analysis, Tech. Rep. SAND2012-2389, Sandia National Laboratories (2012).

[19] M. Lave, J. Kleissl, J. S. Stein, A wavelet-based variability model (WVM) for solar PV power plants, IEEE Transactions on Sustainable Energy PP (99) (2012) 1–9.

[20] M. Lave, J. Kleissl, Cloud speed impact on solar variability scaling–application to the wavelet variability model, Solar Energy 91 (2013) 11–21.

[21] J. Hay, J. Davies, Calculations of the solar radiation incident on an inclined surface, in: Proc. of First Canadian Solar Radiation Data Workshop, 59, Ministry of Supply and Services, Canada.

[22] D. L. King, J. A. Kratochvil, W. E. Boyson, Photovoltaic array performance model, Tech. Rep. SANDIA report SAND2004-3535, Sandia National Laboratories (2004).

[23] D. L. King, S. Gonzalez, G. M. Galbraith, W. E. Boyson, Performance model for grid-connected photovoltaic inverters, Tech. Rep. SANDIA report SAND2007-5036, Sandia National Laboratories (2007).

[24] M. Reno, K. Coogan, Grid integrated distributed PV (Grid PV) version 2, Tech. Rep. SAND2014-20141, Sandia National Laboratories (2014).

[25] J. Quiroz, M. Reno, R. Broderick, Time series simulation of voltage regulation device control modes, in: Photovoltaic Specialists Conference (PVSC), 2013 IEEE 39th, 2013, pp. 1700–1705. doi:10.1109/PVSC.2013.6744472.